CONTRAST MEDIA & MOLECULAR IMAGING
Contrast Med. Mol. Imaging **1**: 153–164 (2006)
Published online 8 August 2006 in Wiley InterScience (www.interscience.wiley.com). DOI:10.1002/cmmi.103

CONTRAST MEDIA & MOLECULAR IMAGING

Full Paper

Tumor imaging in small animals with a combined micro-CT/micro-DSA system using iodinated conventional and blood pool contrast agents

Cristian T. Badea, Laurence W. Hedlund, Ming De Lin, Julie F. Boslego Mackel and G. Allan Johnson*

Center for In Vivo Microscopy, Duke University Medical Center, Box 3302, Durham, NC 27710, USA

Received 23 December 2005; Revised 4 June 2006; Accepted 13 June 2006

ABSTRACT: X-ray based micro-computed tomography (CT) and micro-digital subtraction angiography (DSA) are important non-invasive imaging modalities for following tumorogenesis in small animals. To exploit these imaging capabilities further, the two modalities were combined into a single system to provide both morphological and functional data from the same tumor in a single imaging session. The system is described and examples are given of imaging implanted fibrosarcoma tumors in rats using two types of contrast media: (a) a new generation of blood pool contrast agent containing iodine with a concentration of 130 mg/mL (Fenestra™ VC, Alerion Biomedical, San Diego, CA, USA) for micro-CT and (b) a conventional iodinated contrast agent (Isovue®-370 mg/mL iodine, trademark of Bracco Diagnostics, Princeton, NJ, USA) for micro-DSA. With the blood pool contrast agent, the 3D vascular architecture is revealed in exquisite detail at 100 μm resolution. Micro-DSA images, in perfect registration with the 3D micro-CT datasets, provide complementary functional information such as mean transit times and relative blood flow through the tumor. This imaging approach could be used to understand tumor angiogenesis better and be the basis for evaluating anti-angiogenic therapies. Copyright © 2006 John Wiley & Sons Ltd.

KEYWORDS: micro-computed tomography; micro-angiography; rodents; Fenestra; Isovue; x-ray; tumors

INTRODUCTION

Angiogenesis is a key element of a developing cancer, providing the blood supply to a tumor, which subsequently allows its malignant progression (1,2). Dynamic contrast-enhanced computed tomography (CT) and MRI are used most frequently to evaluate tumor vasculature in patients (3,4). However, imaging the angiogenic circulation in small animals is extremely challenging because the vessels are small and beyond the resolution limits of clinical systems. For *in vivo* studies in rodent models, we must confront not only their small size but also the extremely fast pace of their biological functions. Therefore, imaging tumors in rodents requires dedicated small animal systems. Tumor imaging in rodents is currently performed using several modalities, including MRI (5), micro-CT (6–9), optical (10) and nuclear techniques (11). In some cases, combinations of two modalities are used, for example micro-CT/micro-PET to provide complementary information related to the morphology (micro-CT) and function, i.e. metabolism (micro-PET) (12).

Micro-CT has already been proposed for morphological imaging of vasculature in tumors (9). Obtaining three-dimensional geometric data of vascular systems is possible using micro-CT data and can be valuable to differentiate features of vascular systems in genetic knock-out studies (13). Functional information, such as tumor blood flow, is also very important in tumor assessment. For instance, poor blood flow leads to tissue hypoxia, even in the presence of abundant angiogenesis (14). First-pass perfusion studies in humans require clinical CT systems with a temporal resolution of at least 1 s, i.e. 1 or 1.5 heart beats per image (15). Scaling these temporal requirements to the rodent would require sampling at least every heartbeat, with an inter-scan time on the order of about 150 ms in rats and 100 ms in mice. This is not possible with any of the commercial micro-CT systems currently available. For example, the fastest commercial small animal scanner of which we are aware is the GE eXplore Locus Ultra system (GE Medical Systems, Milwaukee, WI, USA) with a scan time of ∼1 s (16).

The goal in the present work was to design x-ray-based methods and implement them on an instrument capable of

**Correspondence to*: C. T. Badea, Center for *In Vivo* Microscopy, Duke University Medical Center, Box 3302, Durham, NC 27710, USA. E-mail: chris@orion.duhs.duke.edu
Contract/grant sponsor: NCRR/NCI; *contract/grant number:* P41 RR005959/R24 CA-092656.

providing both morphological and functional information related to tumor vasculature in small animals. This goal was achieved by combining micro-CT and micro-DSA in a single system. This paper describes a prototype, combined micro-CT/micro-DSA system that addresses several significant barriers to x-ray imaging in small-animals: (1) the reduced signal-to-noise ratio imposed by the smaller voxels, (2) artifacts from biological motion (17–19) and (3) the need for high temporal resolution. To our knowledge, this is the first system adapted for combined micro-CT/micro-DSA in small animals. The system allows the use of high x-ray photon fluence with integrated physiological monitoring of cardiac motion and control of breathing and with an imaging temporal resolution on the order of ~140 ms. A previous study (18) compared the photon fluence delivered by the present tube with that reported for a microfocal x-ray tube (20) and it was shown that when operating at 80 kV_p, 100 mA the present tube produced an exposure of 70 mR at the detector in a 10-ms exposure or1.53×10^9 photons/mm^2, compared with 2.6×10^7 photons/mm^2 s given by a microfocal x-ray tube operating at 80 kV_p and 0.1 mA. The present tube is capable, however, of operating at 620 mA, i.e. a fluence nearly 250 times greater than the microfocal tubes.

Vascular imaging with x-rays involves the use of contrast agents. Three-dimensional vascular morphology can be provided by micro-CT, but the relatively long scanning time (10–20 min) associated with common micro-CT systems, including ours, require a contrast agent that will ensure a constant enhancement during the scanning interval. This is only possible with a contrast agent that remains in the blood for relatively long periods. For this, a newly developed blood pool contrast agent containing iodine with a concentration of 130 mg/mL (Fenestra™ VC, Alerion Biomedical, San Diego, CA, USA) was used. On the other hand, functional information such as mean transit time and relative blood flow given by micro-DSA required the use of a small molecule freely diffusible conventional iodinated contrast agent (Isovue®-370 mg/mL iodine, trademark of Bracco Diagnostics, Princeton, NJ, USA). We believe that this combined micro-CT/micro-DSA approach could be used to understand tumor angiogenesis and to aid in evaluating anti-angiogenic therapies.

MATERIALS AND METHODS

Imaging systems

The combined micro-CT/micro-DSA system was custom-made and consists of a high-flux rotating anode x-ray tube (SRO 09 50, Philips Medical Systems, Andover, MA, USA) designed for clinical angiography, with a dual 0.3/1.0 mm focal spot operating at 9 kW (0.3 mm focal spot) or 50 kW (1.0 mm focal spot). The detector is a cooled, charge-coupled device camera with a Gd_2O_2S phosphor on a 3:1 fiber optic reducer (X-ray ImageStar, Photonics Science, Robertsbridge, East Sussex, UK). The camera has a 106 mm^2 active field of view with an image matrix of 2048 × 2048 pixels with pixel size of 51 × 51 μm. The tube and detector are mounted in the horizontal plane on aluminum frame components (80/20 Inc., Bellevue, WA, USA) and the animal is held in the vertical position (see Fig. 1), centered in front of the detector face. The distance between the detector and animal is 40 mm and the distance between the animal and x-ray source is 480 mm. This configuration results in a geometric blur of the focal spot that matches the Nyquist sample at the detector (18). Hence this geometry provides a magnification of 1.09, essentially eliminating penumbral blur.

The use of the fixed gantry with the rotating animal has two distinct benefits over traditional commercial scanners. First, it permits the use of larger focal spots, in turn providing a much higher radiation flux. Second, since the mass of the animal is small, this geometry allows a step and shoot rotation with arbitrary intervals, which in turn makes synchronization of the exposure to the physiological state much easier. For micro-DSA imaging, we use a custom-built power micro-injector, which consists of a computer-controlled solenoid valve attached to the contrast injection catheter, heated contrast agent reservoir and power from compressed N_2 (90 psi). This device reproducibly injects volumes down to 6 μL at a rate of 1–2 μL/ms. Isovue is heated to the body temperature, eliminating thermal shock and reducing contrast viscosity. The high power driving the injection is necessary to compensate for the small-caliber lumen and high resistance of the injection catheters (2–3 Fr)

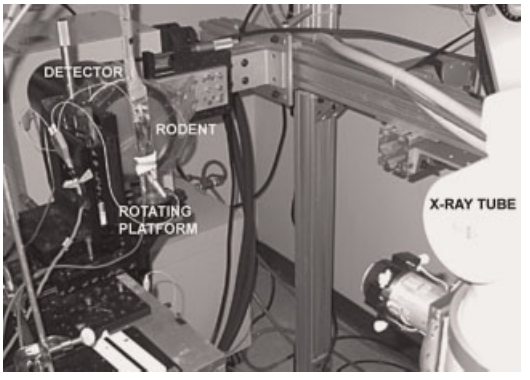

Figure 1. The system in combined micro-CT/DSA configuration. The components of the system are labeled. The X-ray tube and detector are stationary. For a combined micro-CT/micro-DSA study, the rodent is supported in an acrylic tube placed on a support, which is rotated by a computer-controlled stepping motor. The tube and detector are supported on a gantry constructed from extruded aluminum to limit the impact of building vibration. A valve for scan-synchronous ventilation and ECG leads are supported from the top of the gantry. Temperature is maintained using an infrared lamp and a temperature controller. For micro-DSA, the micro-injector injects Isovue 370 heated at the rodent body temperature by a heating controller.

DOI: 10.1002/cmmi

and the high power is also needed to achieve the high flow velocity for bolus injections. To maintain the stable, vertical position for imaging, the rodent is held in an acrylic cradle using an upper incisor bar and the limbs are taped to the side of the cradle. The cradle is then placed on a circular pedestal that is rotated about the vertical axis by a computer-controlled stepping motor (Model 13049, Newport Oriel Instruments, Irvine, CA, USA).

Animal procedures

All animal procedures were approved by the Duke University Institutional Animal Care and Use Committee. A total of ($n = 5$) Fischer 344 rats (Charles River, Raleigh, NC, USA) were imaged, weighing ~175 g, which received subcutaneous implants of 1–2 mm^3 pieces of a rat fibrosarcoma (FSA) in the neck region ($n = 2$) and over the flank of the leg ($n = 3$). The transplantable rat (FSA) tumor line used for this study was originally developed into Fischer 344 rats as described (21). The tumor line does not grow *in vitro*, so it is maintained by serial transplantation.

Tumors were imaged 3 weeks after implantation after reaching a diameter larger than 15 mm. The rats were initially anesthetized with a 50 mg/kg intraperitoneal injection of sodium pentobarbital and 2 mg/kg butorphanol (Fort DodgeAnimal Health, Fort Dodge, IA, USA) and then perorally intubated (18 gauge Intracath) for mechanical ventilation. For ventilation, a pneumatically powered breathing valve was connected directly to the endotracheal tube (22). This valve also contained a pressure transducer for monitoring airway pressure. Breathing-air power hoses and pressure transducer leads were tethered to the gantry above the rat head in a manner allowing free rotation. During imaging, anesthesia was maintained with 1–2% isoflurane (Halocarbon, River Edge, NJ, USA) delivered by the ventilator. ECG was monitored using electrodes taped to footpads and body temperature was recorded using either an oral thermistor for rats with leg tumors or a rectal thermistor for rats with neck tumors. In these positions, the thermistor wires would not be in the field of view to produce image artifacts. The flexible tubes and wires carrying anesthesia gas and physiological signals were suspended from above to allow free rotation during scanning. Coulbourn modules (Coulbourn Instruments, Allentown, PA, USA) processed the physiological signals, which were then displayed on a computer monitor using a custom LabVIEW application (National Instruments, Austin, TX, USA). Body temperature was recorded and maintained at 37°C by heat lamps and a feedback controller system (Digi-Sense, Cole Parmer, Chicago, IL, USA).

For micro-DSA imaging of leg tumors, a 2F catheter for contrast injection was inserted into the contra-lateral common iliac artery, and for the neck tumors, the injection catheter was placed in the right common carotid artery with the tip just above the branch of the right subclavian artery. For micro-CT imaging, the same catheters were used for the injection of Fenestra VC.

Imaging procedures

To minimize blurring effects of biological motion and to synchronize image capture to breathing and cardiac cycles, a computerized event controller was used that incorporated physiological signals (cardiac, breathing) to control events such as x-ray exposure, camera acquisition, contrast injection (timing and volume) for micro-DSA and animal rotation for micro-CT. This biological pulse sequence controller is a custom LabVIEW application (National Instruments) and is illustrated schematically in Fig. 2. A typical study was done in two steps: first micro-CT, then micro-DSA.

For micro-CT, precise event control is necessary to ensure that any single projection obtained using millisecond exposures (<10 ms), is synchronized exactly to particular phases of both the cardiac and breathing cycles (23). The control sequence incorporates prospective cardio-respiratory gating [see Fig. 2(A)]. With micro-CT, a newly developed blood pool agent, Fenestra VC, was

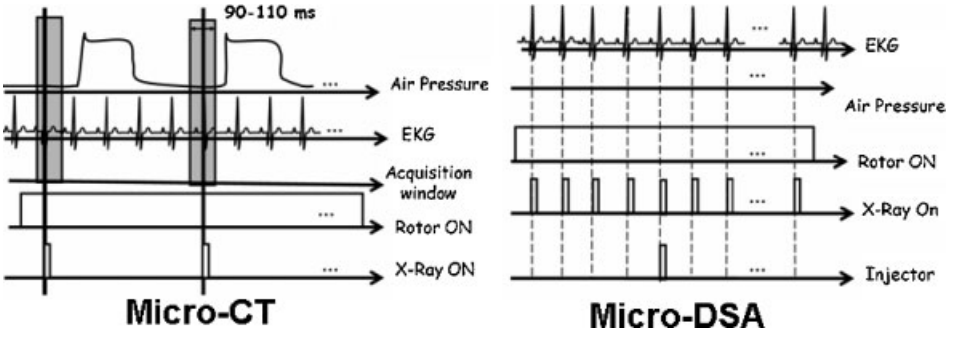

Figure 2. The micro-CT and micro-DSA biological pulse sequences. In micro-CT, the sampling is performed at end-expiration and on the QRS complex. Any QRS occurring within the window placed at end-expiration triggers an X-ray exposure. The micro-DSA gating sequence is used to sample in suspended respiration (10–12 s) and is synchronized with the cardiac cycle. Pre-contrast injection and post-contrast injection images are taken every cardiac cycle.

DOI: 10.1002/cmmi

used, consisting of iodinated triglycerides formulated in a stable, sub-μm oil-in-water lipid emulsion (24,25) containing 130 mg/mL iodine. Following injection of 1.25 mL of Fenestra VC, an image was acquired every breath at end-expiration during a period $<$ R–R beat to beat interval and synchronous with the ECG QRS complex. The animal was then rotated to the next angle. Typically a full image dataset covered 190° in 0.5° steps for a total of 380 projections. We use a rotation of 190° (i.e. 180° + fan angle) instead of 360° to reduce the problems associated with the twisting of tubes and cables. The x-ray settings were 80 kV_p, 170 mA and 9 ms. Each projection was taken using cardio-respiratory synchronization, i.e. at end expiration and cardiac gated. The total scan time for a micro-CT dataset is on average 15 min. Dosimetric measurements were performed using a Wireless Dosimetry System Mobile MOSFET TN-RD-16, SN 63 (Thomson/Nielsen, Ottawa, ON, Canada). Five MOSFET dosimeter silicon chips (1 mm^2 active area 0.2 mm × 0.2 mm) were positioned at the surface and the center of a rodent-like phantom made out of acrylic. During micro-CT scanning, the measured dose was ∼22 cGy. Projections were used to reconstruct tomograms with a Feldkamp algorithm using Parker weighting (26). The Cobra EXXIM software package (EXXIM Computing, Livermore, CA, USA) was used. Data were reconstructed as isotropic 1024 × 1024 × 1024 arrays with effective digital sampling in the image plane of 100 μm. The injection of 1.25 mL of Fenestra VC added 165 mg of iodine to the blood pool and produced an enhancement relative to the non-contrast dataset of ∼518 Hounsfield Units (HU) in the blood measured in the left ventricle.

Following micro-CT, the micro-injector was connected to the appropriate catheter and the micro-DSA was performed with injections of Isovue 370 (370 mg I/mL), a conventional iodinated contrast agent, using the control sequence described in Fig. 2(B).

During micro-DSA imaging, the animals were kept in suspended respiration at end-expiration for 10 s to eliminate breathing motion artifacts. Heart rates did not change during the periods of suspended breathing. Images were acquired synchronous with the QRS complex. First, five pre-contrast images were acquired to serve as a mask, then a 150 μL bolus of Isovue 370 contrast was injected over 300 ms, followed by a series of post-contrast images that were also acquired at every heartbeat triggered by the QRS complex. The pre-contrast images were averaged to create a mask that was logarithmically subtracted from each post-contrast image. This yields a digital subtraction angiography series from which functional metrics can be derived. The temporal resolution for these DSA studies was one image per heartbeat (every 140 ms) with an in-plane spatial resolution of 100 μm. Although the actual acquisition time is about 10 ms, images can only be repeated every 140 ms because of the delays due to data readout from the camera. The x-ray settings were 80 kV_p, 250 mA and 9 ms and the estimated dose was about 3.4 cGy for a set of 40 images. Thus, for the complete imaging session of micro-CT and micro-DSA, the total radiation dose that each animal received was about 25.4 cGy. After processing, the public domain software ImageJ (National Institute of Health, Bethesda, MD, USA) was used to render the minimum and maximum intensity projections and to analyze the data.

Flow analysis

Micro-DSA images contain functional information related to blood kinematics that can be extracted using the analysis of the time–density curves. The intravascular phase of contrast enhancement was used to evaluate perfusion, i.e. blood flow per unit volume or mass of tissue. This parameter is generally increased in tumors (15). To evaluate mean transit times, regions of interest (ROIs) of ∼30 pixels were selected in the vessels by manually drawing on the micro-DSA images and mean intensity values from these ROIs were plotted over time. A gamma variate function was then fitted (27–29) to the mean values of the ROIs using a non-linear least-squares fit. The nonlinear data-fitting provided by *lsqnonlin* implemented in the mathematical program MATLAB (v. 5 for Windows 95/NT, The MathWorks, Natick, MA, USA) was used as the function that fits the gamma variate to the data. As a measure of errors in fitting, R^2 is given. The R^2 value is the square of the correlation coefficient and gives a measure of the reliability of the fitting.

The contrast agent concentration, $C(t)$, at time t is expressed as

$$C(t) = C_p(e/\alpha\beta)^{\alpha}(t - AT)^{\alpha}e^{-(t-AT)/\beta}$$

where t is the time after contrast injection, C_p is the peak concentration, AT is the appearance time and α and β are fitting parameters.

From the fitted curve, the hemodynamics parameters mean transit time (*MTT*) and relative flow (*RF*) were derived:

$$MTT = AT + \beta(\alpha + 1) = \frac{\int tC(t)dt}{\int C(t)dt}$$

$$RF = \frac{1}{MTT}$$

i.e. blood flow per unit vascular volume.

The *MTT* and *RF* values provide information on the regional transit time and flow of contrast agent through the vessels.

RESULTS

Figure 3 shows micro-CT images of an FSA tumor implanted in the neck region. The 3D vascular architecture

DOI: 10.1002/cmmi

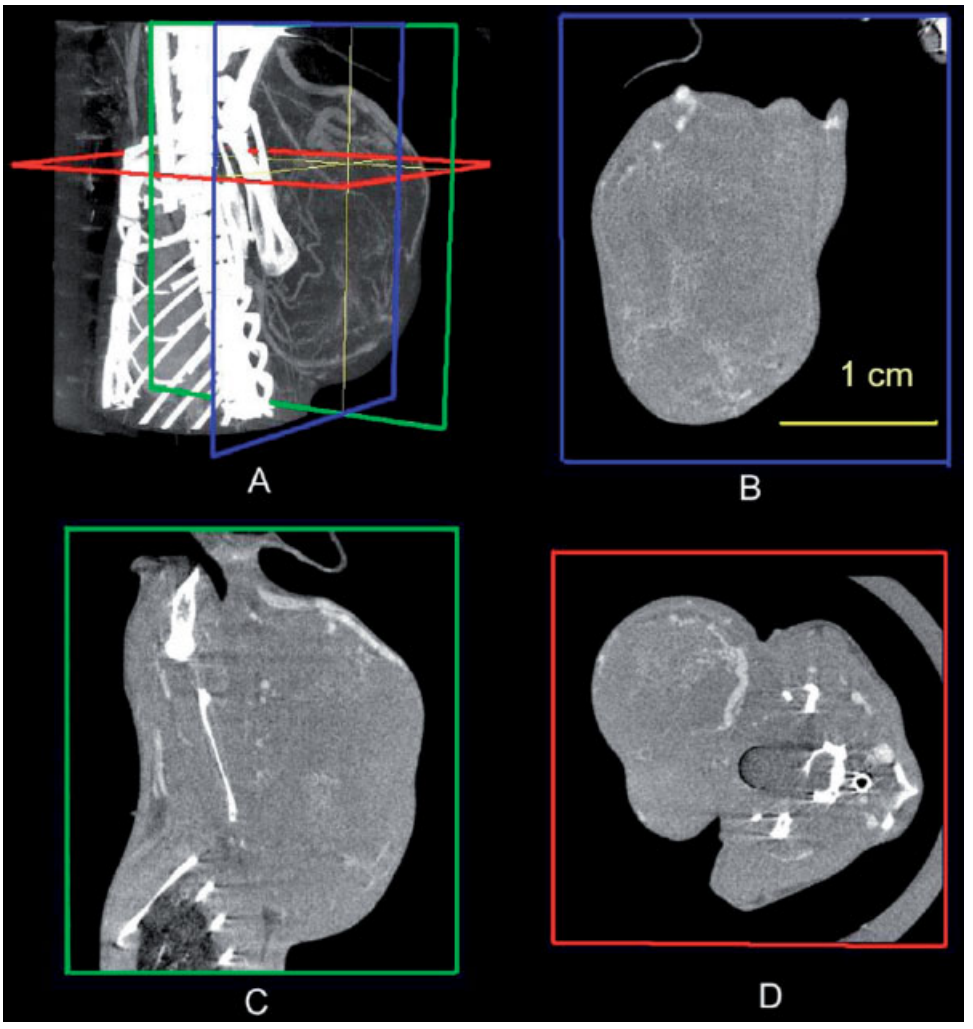

Figure 3. Micro-CT imaging of a neck implanted FSA tumor with Fenestra VC blood pool contrast agent: (A) volumetric maximum intensity projection rendering and three orthogonal slices through the tumor in coronal (B) sagittal (C) and axial orientations.

is most apparent in the maximum intensity projection (MaxIP) rendering shown in Fig. 3(A). Since it is difficult to appreciate the 3D nature of the tumor in a single image, we show the tumor in three orthogonal planes [Fig. 3(B)–D)]. The tumor appears as a bi-lobed mass with the central portion being poorly vascularized. From the micro-CT orthogonal images [Fig. 3(B)–D)], the tumor vessels appear to have a diameter in the range 100–300 μm. The micro-DSA images [Fig. 4(A) and (B)] were obtained after a single bolus injection of contrast into the common carotid artery and show the dual arterial supply to the tumor. Arterial and venous separation is not clearly apparent in the micro-CT images where they are equally enhanced. One can also appreciate that the injection was timed to occur during ventricular diastole as the aortic valve is closed. The presence of myocardial enhancement suggests contrast flow in the coronary arteries [Fig. 4(C) and (D)]. Also apparent is that the arterial supply to the tumor is entirely from the left-side arteries [Fig. 4(A) and (B)]; the branch of the left external carotid artery enhances the peripheral, cranial region of the tumor and a branch from left auxiliary axillary artery supplies the central-caudal region. The persistent, diffuse-contrast enhancement in the tumor mass [Fig. 4(C) and (D)] reflects relatively weak capillary/tissue level perfusion. An enlarged view of the tumor in Fig. 4 is shown in Fig. 5 as the micro-CT maximum intensity projection (MaxIP) [Fig. 5(A)] and micro-DSA temporal minimum intensity projection (MinIP) [Fig. 5 (B)]. We created the micro-DSA MinIP by selecting minimum pixel values (maximum peak enhancement in absolute value) along the time dimension. The comparison of these two images suggests that vascularization is predominately peripheral; this is verified by examination of the axial views from micro-CT plane shown in Fig. 3(D).

Figure 6 shows micro-CT images through an FSA tumor implanted on the flank of the left leg both as MaxIP rendering [Fig. 6(A)] and in three orthogonal planes

DOI: 10.1002/cmmi

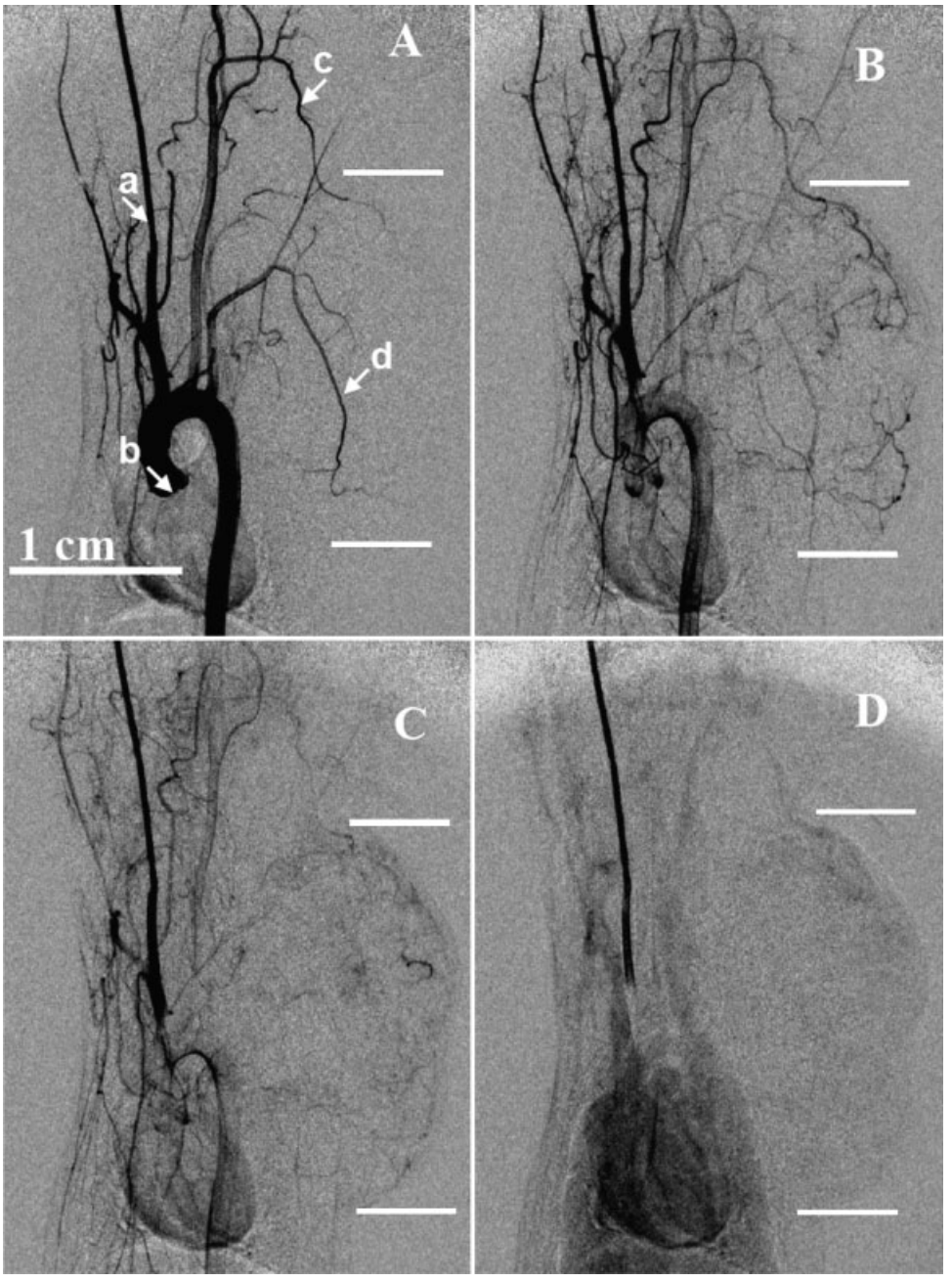

Figure 4. Selected micro-DSA images of a neck FSA tumor positioned between the two lines at 1 (A), 2 (B), 3 (C) and 18 (D) heartbeats post- contrast injection. The vascular anatomy is indicated by arrows as follows: right carotid and catheter (a), aortic valve (b), branch from external left carotid (c) and branch from axillary artery (d). There appears to be two major arterial blood supplies to the tumor: the left external carotid artery (c) and the branch from the left axillary artery (d).

[Fig. 6(B–D)]. The relatively little contrast enhancement seen here suggests a poorly vascularized tumor with predominately peripherally arranged arterial supply. The source of the arterial supply to the tumor is seen in the micro-DSA images (Fig. 7). These images are selected from a beat-to-beat series of images after a single bolus contrast injection in to the right common iliac artery. In contrast to the carotid artery injection for the neck tumor, the main phase of arterial flow into this flank tumor is delayed by one beat because of the significant retrograde flow in the abdominal aorta. However, this retrograde aortic flow serves to reveal one of the arterial supplies to the tumor, that being from the iliolumbar artery, which is a branch of the aorta near the left kidney [Fig. 7(B) and (C)]. Arterial supply also comes from the left common iliac artery. These four post-contrast micro-DSA images were acquired in the same FSA leg tumor as shown in Fig. 6, at heartbeats 2 (A), 6 (B), 9 (C) and 16 (D) post-contrast

DOI: 10.1002/cmmi

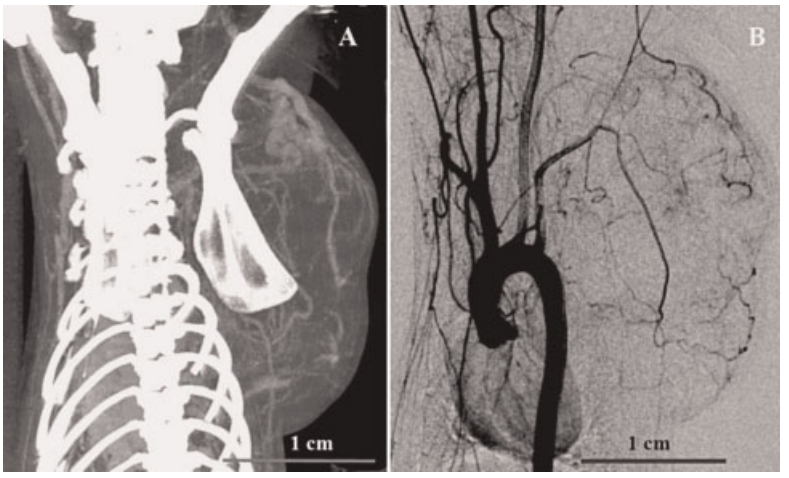

Figure 5. Comparison of and micro-CT maximum intensity projection (A) and micro-DSA temporal minimum intensity projection (B) for the neck FSA tumor.

injection. Note how the dynamic images show both the arrival of the bolus through one artery [arrow in Fig. 7(B)] followed by tumor perfusion and the return of the contrast bolus through the veins [arrow in Fig. 7(D)].

The late enhancement [Fig. 7(D)] of the tumor suggests capillary filling and venous flow. This contrast injection compared with the carotid injection is more concentrated, especially to the lower abdomen, tail and left leg [Fig. 7(D)]. Several veins are visible at this stage, such as caudal vena cava, common iliac, femoral and external iliac. The vascular architecture of the tumor is made clearer by side-by-side comparisons of micro-CT MaxIP and micro-DSA temporal MinIP during arterial flow as shown in Fig. 8. Areas of diffuse contrast enhancement seen in the micro-DSA [Fig. 8(B)] correspond roughly to the areas of more intense vascularization seen in the micro-CT image [Fig. 8(A)]. However, it is clear that the enhancement seen in the micro-DSA, being dynamic, generally appears weaker because the contrast agent is diluted by flow of unopacified blood into the tumor, whereas with micro-CT, the long half-life of the blood pool agent maintains a persistently high level of attenuation of both arteries and veins.

To estimate blood flow through the same FSA leg tumor as shown in Fig. 8, samples were taken from three ROIs [see Fig. 9(A)]. ROI 1 covers the common iliac artery and vein and samples circulation to the lower leg and tumor. ROI 2 samples from an intra-tumor artery superimposed with a vein and ROI 3 samples from the peripheral region of the tumor. The time–density curves for each region and the fitted gamma variate functions are shown in Fig. 9(B). The first peak from ROI 1 reflects the initial peak arterial inflow through the iliac artery to the lower leg and tumor followed by the second smaller peak representing iliac vein venous return primarily from the lower leg. ROI 2 represents the initial arterial input to this part of the tumor and its peak is slightly delayed from the systemic arterial supply. This is followed by a second smaller peak representing venous return from the tumor. Finally, the peripheral enhancement represented by ROI 3 is greatly reduced compared with the other two regions due primarily to contrast dilution. Table 1 shows the values of *MTT* and *RF*. Although at this level we do not have ways to calibrate and validate the hemodynamics information, note that the largest vessel (ROI 1) shows the largest *RF* and the shortest *MTT*. The opposite is true for the ROI 3, the smallest of the selected vessels.

DISCUSSION AND CONCLUSIONS

This paper presents x-ray methods and instrumentation for tumor imaging in small animals using both conventional and blood pool contrast agents. The system design involves animal rotation in a vertical position, which can be argued as being unnatural. The influence of a vertical body position on murine systemic blood pressure and left ventricular (LV) hemodynamics over time has been investigated with MR microscopy (30). After tilting, there was a transient decrease in LV systolic pressure to 96% of initial values immediately after tilting with return to baseline level within 6 min. Tilting to vertical position had no influence on LV end-diastolic pressure, heart rate, maximum rate of LV pressure increase and maximum rate of LV pressure decrease. Hence it is believed that vertical position is not a major drawback in the present approach. The main application goal was to provide morphological and functional information in a tumor and not to use the system for tumor detection. Preclinical imaging with micro-CT in rodents clearly benefits from the use of blood pool contrast agents able to encapsulate a high concentration of iodine. The highly iodine concentrated Fenestra VC,

DOI: 10.1002/cmmi

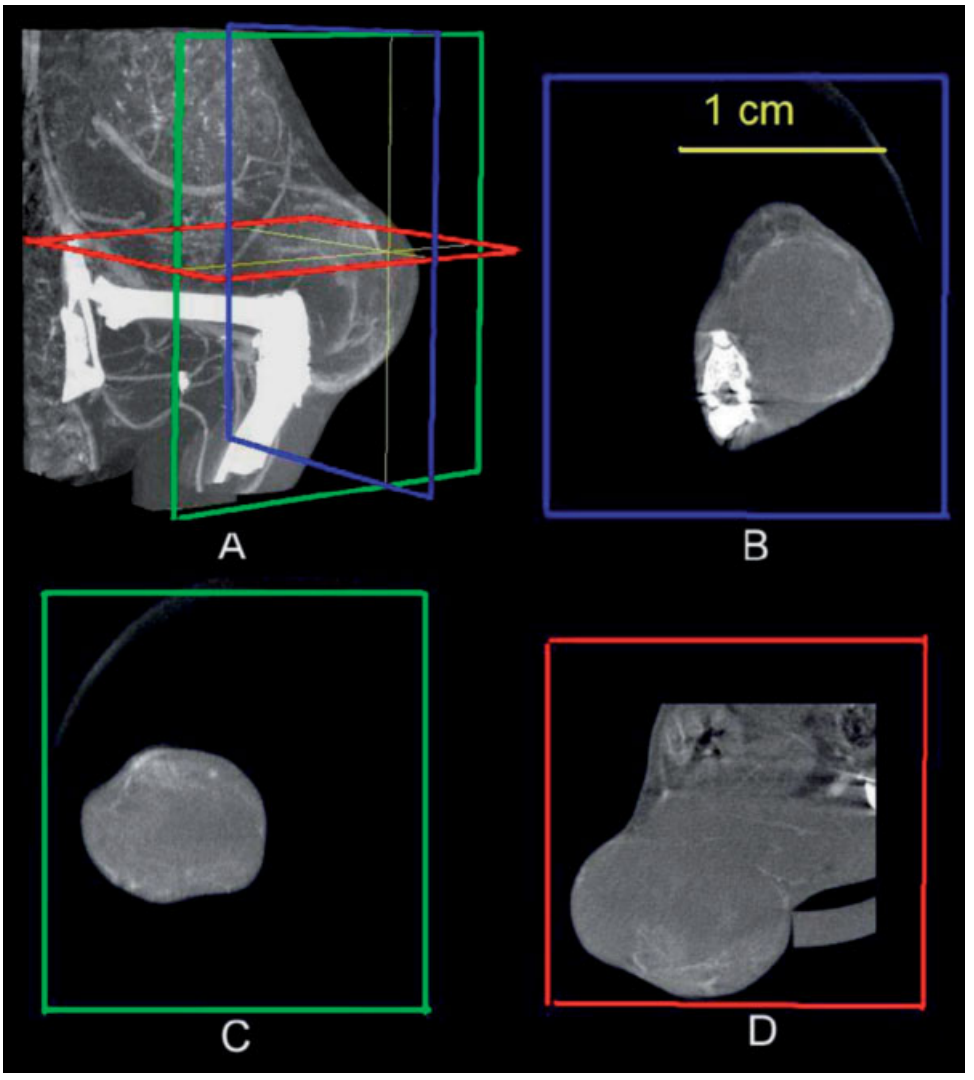

Figure 6. Micro-CT imaging of a leg implanted FSA tumor with Fenestra VC blood pool contrast agent: (A) volumetric maximum intensity projection rendering and three orthogonal slices through the tumor in coronal (B) sagittal (C) and axial orientations.

containing 130 mg I/mL, relative to the commercially available Fenestra VC with 50 mg I/mL, has the benefit of reducing the dose injected for the same enhancement. Alternatively, increasing the iodine concentration and keeping the same dose increases the opacity and the chances to visualize very thin vessels present in the tumors. Indeed, a comparison of micro-DSA temporal MinIP and the MaxIP image from micro-CT data (Figs (5) and (8)) shows finer vasculature in the micro-DSA image using Isovue. This is not surprising, since the modulation transfer function (MTF) at 10% value for this micro-CT system is close to 3 lp/mm (18). Therefore, the blurring is larger than in the single projection image. On the other hand, the micro-CT images show no difference between the arteries and veins, whereas in micro-DSA the veins (larger) in the imaged tumors are not well visualized owing to the contrast dilution. Additionally, arteries and veins can be distinguished based on the time sequence of contrast flow with arteries appearing first and the veins later.

The sequential use of two different contrast agents in the same animal could have the potential for undesirable interactions and adverse reactions; however, no changes related to this combination of agents in the animals were noticed. Also, the highly lipophilic nature of the core of Fenestra VC particles argues against any interaction with a water-soluble agent such as Isovue 370.

Cardio-respiratory gating used in these studies successfully minimizes the blurring effects of cardiac and breathing motion and aids in maintaining maximum spatial resolution of micro-CT images. This is especially true for imaging of the neck, thorax and upper abdomen. Although image comparisons between gated and non-gated images are not shown, the clarity and spatial

DOI: 10.1002/cmmi

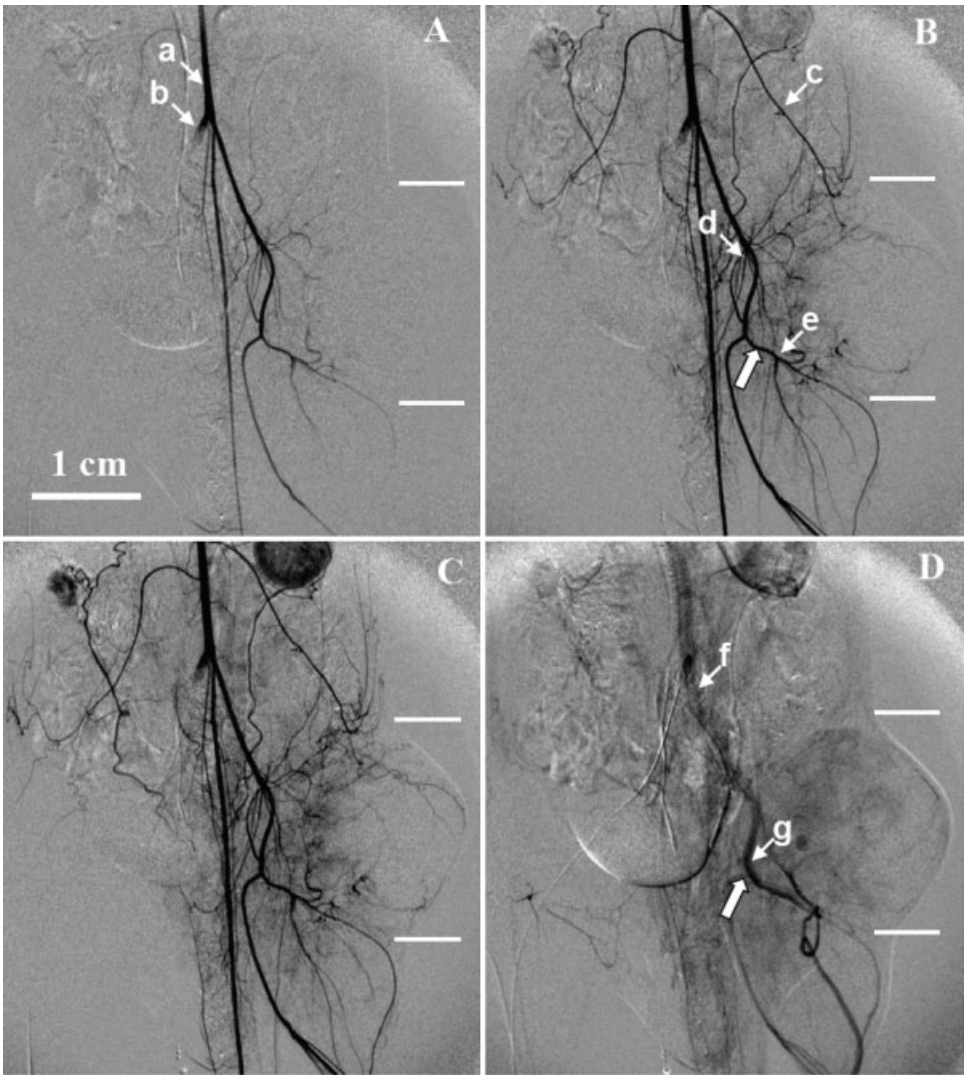

Figure 7. Selected micro-DSA images of the FSA tumor (positioned between the two lines) at 2 (A), 6 (B), 9 (C) and 18 (D) heartbeats post-contrast injection. The large arrow in (B) indicates one of the vessels doing the arterial feeding, i.e. the external iliac artery, while the large arrow in (D) shows the venous return of the bolus from the lower leg. The vascular anatomy is indicated by arrows: abdominal aorta (a), common iliac artery (b), iliolumbar artery (c), external iliac artery (d), femoral artery branch (e), caudal vena cava (f) and external iliac vein (g). There appear to be three primary arterial blood supplies to the tumor: iliolumbar artery (c), branch from external iliac (d) and femoral artery branch (e).

resolution evident in the example of images of the neck tumor [Figs (4) and (5)(B)] demonstrate the effectiveness of these gating methods in controlling effects of motion. Furthermore, in a recent publication (31), it was shown that without gating, the errors associated with motion of the lungs (and thus presumably in tumors placed over the thorax) could be on the order of a few millimeters. Imaging regions distant from the lungs and heart, such as the lower abdomen and legs, is far less problematic in relation to motion control and does not strictly require gated imaging. However, for the sake of methodological consistency, it is preferred to use gating for all *in vivo* imaging studies. This also has the added benefit of allowing the use of inhalational anesthetics such isoflurane, which are far easier to control than injectables and are easily delivered by mechanical ventilation using a endotrachial tube. Peroral intubation does not damage the trachea and animals anesthetized with isoflurane are easily recovered in the case of longitudinal studies.

Breathing motion issues for micro-DSA imaging were addressed successfully by imaging during suspended breathing. However, the micro-DSA studies highlighted several other challenges related to the position (neck or leg flank) of the implanted tumor. One challenge is the position of the contrast agent catheter in relation to the tumor. This position is critical for identifying the tumor's arterial supply (Fig. 7). Since in the neck region this supply might come from arteries on both right and left

DOI: 10.1002/cmmi

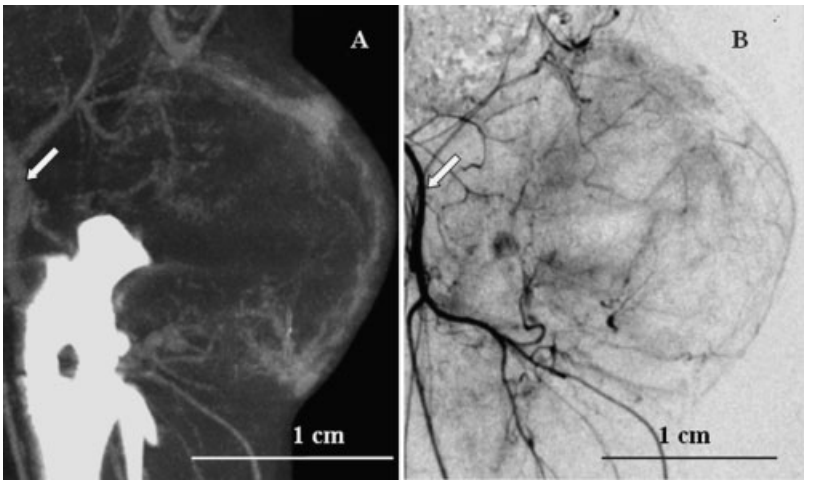

Figure 8. Comparison of micro-CT maximum intensity projection (A) and micro-DSA temporal minimum intensity projection during arterial flow phase (B) for the leg FSA tumor shown in Fig. 7. Vascular profiles shown by arrows appear thicker in (A) than in (B) because the external iliac artery and vein are very close together and are both seen in (A), but only the artery is seen in (B).

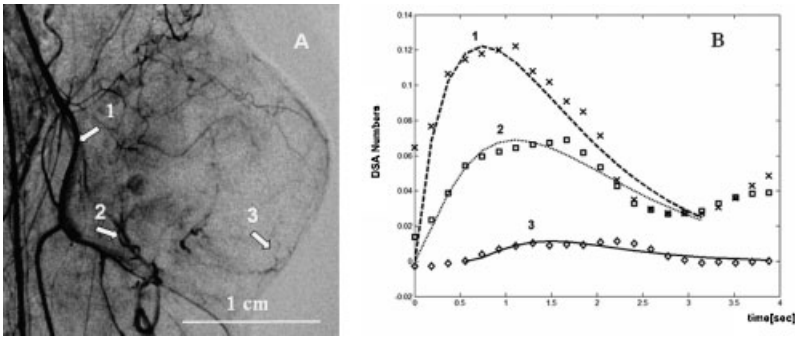

Figure 9. Mean transit times and relative blood flow are assessed in the leg-implanted FSA tumor, as shown in Figs. 7 and 8, in three ROIs (A) by analyzing the time–density curves fitted using gamma variates (B).

sides, placement of the catheter on one side could conceivably block some vessels supplying the tumor, hence these vessels would not be seen. On the other hand, a tumor placed on the mid-portion of the flank of the thigh will be supplied by arteries on the same side. Thus, a contrast injection catheter placed in the contralateral leg or in the abdominal aorta is very likely to provide complete visualization of the tumor's arterial supply. Another issue with DSA of neck versus leg tumors is that blood flow in the neck occurs at much higher velocity owing to the proximity of the heart than flow in the leg (compare Fig. 4 with Fig. 8). The temporal resolution of image acquisition is much more critical for neck than for leg tumors.

Since DSA is a planar method, quantitative measurements are difficult because of overlap of non-homogeneous x-ray attenuating structures such as vessels. This problem is even worse with large structures containing

Table 1. The mean transit times (*MTT*) and relative flow (*RF*) computed for the three ROIs selected in three vessels in the micro-DSA data; the accuracy of the fitting is characterized by the correlation coefficient R^2

	MTT (s)	*RF* (s^{-1})	R^2
ROI 1	1.575	0.63	0.95
ROI 2	1.818	0.55	0.90
ROI 3	1.938	0.51	0.98

DOI: 10.1002/cmmi

contrast or in situations where blood flow is low. However, with careful timing, physiological motion control and optimized injection characteristics, ROIs can be chosen without overlapping structures. This temporal selection is illustrated by the time-density curve for vessel 1 [Fig. 9(A)] displaying a second peak of enhancement. This corresponds to the vein enhancement spatially overlapping in the same region [see the arrows in Fig. 7(B) and (D)]. It is important to note that the second peak enhancement is not the result of recirculation, since this does not occur in the temporal range of the scanning time. Furthermore, a bolus of 150 μL of contrast agent would be greatly diluted after recirculation and would probably not be detected. By carefully selecting the time points in the fitting of the gamma variate function, one can select only the arterial phase. However, overlapping vessels are a real problem for micro-DSA and work is under way to apply a limited angle imaging method based on tomosynthesis to provide depth discrimination (32). Tomosynthesis augments a projection imaging method such as DSA by providing 3D information through a series of coronal slice images eliminating the problem of overlapping structures. For measurements of absolute values in blood flow, further work with phantoms would be required (33).

The experiments shown here were not designed as a survival study, but longitudinal studies are possible with micro-CT/micro-DSA, especially if rodents with indwelling catheters are used.

Although this report only includes images and data over a relatively small number of animals, the same methods have been used over the past 2 years involving more than 50 rats and mice in studies of the cardiopulmonary system.

In conclusion, this study introduces a combined micro-CT/micro-DSA system and demonstrates its use in small animal imaging. An advantage of this approach is that both anatomies, 3D vascular architecture using micro-CT with blood pool contrast agent and functional information using micro-DSA with conventional contrast agent, are obtained in the same animal and a single imaging session. This imaging approach could be used to understand tumor angiogenesis better and to be the basis for evaluating anti-angiogenic therapies.

Acknowledgements

We are grateful to Dr Douglas Bakan of Alerion Biomedical for making the Fenestra™ contrast agent available and for numerous helpful suggestions. We would like to thank Dr Hong Yuan, Dr Yulin Zhao and Dr Mark Dewhirst (Duke Radiation Oncology) for the tumor transplant. We acknowledge the work of Dr Terry Yoshizumi, Greta Toncheva and Giao Nguyen (Duke Radiology) for dosimetric measurements. We also thank Srinivasan Mukundan (Duke Radiology) for useful comments on the manuscript and Sally Zimney for editorial work. All work was performed at the Duke Center for In Vivo Microscopy, an NCRR/NCI National Resource (P41 RR005959/R24 CA-092656).

REFERENCES

1. Folkman J. Tumor angiogenesis: therapeutic implications. *N. Engl. J. Med*. 1971; **285**: 1182–1186.
2. Folkman J. New perspectives in clinical oncology from angiogenesis research. *Eur. J. Cancer* 1996; **32**: 2534–2539.
3. Zhang M, Kono M. Solitary pulmonary nodules: evaluation of blood flow patterns with dynamic CT. *Radiology* 1997; **205**: 471–478.
4. Barentsz JO, Engelbrecht M, Jager GJ, Witjes JA, de LaRosette J, van Der Sanden BP, Huisman HJ, Heerschap A. Fast dynamic gadolinium-enhanced MR imaging of urinary bladder and prostate cancer. *J. Magn. Reson. Imaging* 1999; **10**: 295–304.
5. Benjaminsen IC, Graff BA, Brurberg KG, Rofstad EK. Assessment of tumor blood perfusion by high-resolution dynamic contrast-enhanced MRI: a preclinical study of human melanoma xenografts. *Magn. Reson. Med*. 2004; **52**: 269–276.
6. Ritman EL. Molecular imaging in small animals–roles for micro-CT. *J. Cell. Biochem. Suppl*. 2002; **39**: 116–124.
7. Jorgensen SM, Demirkaya O, Ritman EL. Three-dimensional imaging of vasculature and parenchyma in intact rodent organs with X-ray micro-CT. *Am. J. Physiol*. 1998; **275**: H1103–H1114.
8. Paulus MJ, Gleason SS, Kennel SJ, Hunsicker PR, Johnson DK. High resolution X-ray computed tomography: an emerging tool for small animal cancer research. *Neoplasia* 2000; **2**: 62–70.
9. Kiessling F, Greschus S, Lichy MP, Bock M, Fink C, Vosseler S, Moll J, Mueller MM, Fusenig NE, Traupe H, Semmler W. Volumetric computed tomography (VCT): a new technology for non-invasive, high-resolution monitoring of tumor angiogenesis. *Nat. Med*. 2004; **10**: 1133–1138.
10. Choy G, Choyke P, Libutti SK. Current advances in molecular imaging: noninvasive *in vivo* bioluminescent and fluorescent optical imaging in cancer research. *Mol. Imaging* 2003; **2**: 303–312.
11. Herschman HR. Micro-PET imaging and small animal models of disease. *Curr. Opin. Immunol*. 2003; **15**: 378–384.
12. Jan ML, Chuang KS, Chen GW, Ni YC, Chen S, Chang CH, Wu J, Lee TW, Fu YK. A three-dimensional registration method for automated fusion of micro PET–CT–SPECT whole-body images. *IEEE Trans. Med. Imaging* 2005; **24**: 886–893.
13. Marxen M, Thornton MM, Chiarot CB, Klement G, Koprivnikar J, Sled JG, Henkelman RM. MicroCT scanner performance and considerations for vascular specimen imaging. *Med. Phys*. 2004; **31**: 305–313.
14. McDonald DM, Choyke PL. Imaging of angiogenesis: from microscope to clinic. *Nat. Med*. 2003; **9**: 713–725.
15. Miles KA. Perfusion CT for the assessment of tumour vascularity: which protocol? *Br. J. Radiol*. 2003; **76** Spec. No. 1: S36–S42.
16. Doodewaard SV, Lee T-Y, Holdsworth DW. *Dynamic high-resolution volumetric CT Imaging of tumours in mice*. 2005.
17. Badea CT, Hedlund LW, Wheeler CT, Mai W, Johnson GA. Volumetric micro-CT system for *in vivo* microscopy. Arlington, VA, 15–18 April 2004; 1377–1381.
18. Badea CT, Hedlund LW, Johnson GA. Micro-CT with respiratory and cardiac gating. *Med. Phys*. 2004; **31**: 3324–3329.
19. Lin M, Badea CT, Johnson GA. *Functional cardio-pulmonary imaging of the rodent using micro radiography*. Academy of Molecular Imaging Annual Meeting, Orlando, FL, 2005.
20. Ford NL, Thornton MM, Holdsworth DW. Fundamental image quality limits for microcomputed tomography in small animals. *Med. Phys*. 2003; **30**: 2869–2877.
21. Grant JP, Wells SA Jr. Tumor resistance in rats immunized to fetal tissues. *J. Surg. Res*. 1974; **16**: 533–540.
22. Hedlund LW, Johnson GA. Mechanical ventilation for imaging the small animal lung. *ILAR J*. 2002; **43**: 159–174.

23. Badea C, Fubara B, Hedlund L, Johnson G. 4D micro-CT of the mouse heart. *Mol. Imaging* 2005; **4**: 110–116.
24. Weichert JP, Lee FT J, Longino MA, Chosey SG, Counsell RE. Lipid-based blood pool CT imaging of the liver. *Acad. Radiol*. 1998; **5**: S16–S19.
25. Weichert JP, Bjorling DE, Moser AR, Durkee BY, Longino MA, Lee FTJ. *Virtual MicroCT Angiography with BP20 in live mice*. San Francisco, CA, 15–18 August 2003.
26. Feldkamp LA, Davis LC, Kress JW. Practical cone-beam algorithm. *J. Opt. Soc. Am*. 1984; **1**: 612–619.
27. Thompson HK Jr, Starmer CF, Whalen RE, McIntosh HD. Indicator transit time considered as a gamma variate. *Circ. Res*. 1964; **14**: 502–515.
28. Starmer CF, Clark DO. Computer computations of cardiac output using the gamma function. *J. Appl. Physiol*. 1970; **28**: 219–220.
29. Davenport R. The derivation of the gamma-variate relationship for tracer dilution curves. *J. Nucl. Med*. 1983; **24**: 945–948.
30. Wiesmann F, Neubauer S, Haase A, Hein L. Can we use vertical bore magnetic resonance scanners for murine cardiovascular phenotype characterization? Influence of upright body position on left ventricular hemodynamics in mice. *J. Cardiovasc. Magn. Reson*. 2001; **3**: 311–315.
31. Mai W, Badea CT, Wheeler CT, Hedlund LW, Johnson GA. Effects of breathing and cardiac motion on the spatial resolution in microscopic imaging of rodents. *Magn. Reson. Med*. 2005; **533**: 858–865.
32. Badea C, Kolitsi Z, Pallikarakis N. Image quality in extended arc filtered digital tomosynthesis. *Acta Radiol*. 2001; **42**: 244–248.
33. Rozenn Le G, Yves JB. Densitometric measurement of blood flow application to stenosis quantification. In Murray HL (ed.). *SPIE*, 1992; 378–385.

DOI: 10.1002/cmmi